



Letter to the Editors

# SIMS imaging analyses of in-reactor irradiated boron carbide control rod samples

O. Gebhardt \*, D. Gavillet

*Paul Scherrer Institut, CH-5232 Villigen PSI, Switzerland*

Received 1 December 1999; accepted 22 December 1999

---

**Abstract**

The relative radial burnup of the isotope  $^{10}\text{B}$  in an absorber rod has been determined by cross-sectional imaging analysis using a shielded secondary ion mass-spectrometer (SIMS). Two-dimensional secondary ion images of the specimen cross-section were recorded. The count rates of the burnable isotope  $^{10}\text{B}$  were normalised with the count rates of the non-burnable isotope  $^{11}\text{B}$ . The relative radial burnup of the isotope  $^{10}\text{B}$  was calculated and graphically plotted in the form of 2D-images and vector diagrams. © 2000 Elsevier Science B.V. All rights reserved.

---

**1. Introduction**

In light water nuclear power reactors (LWRs), control rods filled with boron carbide powder in the form of  $\text{B}_4\text{C}$  (or alternatively  $\text{B}_5\text{C}$ ,  $\text{B}_{6,5}\text{C}$ ,  $\text{B}_{8,5}\text{C}$  within its homogeneity range) are most commonly used for neutron absorption during the control and the shut-down. Because of its high neutron absorption efficiency, low neutron induced activity, high melting point and low cost  $\text{B}_4\text{C}$  is an attractive absorber material. However, due to the formation of helium atoms under neutron radiation by the  $^{10}\text{B}(\text{n},\alpha)^7\text{Li}$  nuclear reaction a swelling of the  $\text{B}_4\text{C}$  powder occurs which induces cracks in the claddings of the control rods and reduces their lifetime [1–4].

Different authors have studied the mechanical behaviour, the creation of helium bubbles, the migration of lithium and the microstructure of irradiated  $\text{B}_4\text{C}$  control rods [2–6], but the radial distribution of the boron isotopes and the burnup characteristics of in-reactor irradiated  $\text{B}_4\text{C}$  control rods are not yet known. Applying in a thermal reactor a control material with a large thermal neutron capture cross-section leads to an inhomogeneous radial burnout of the relevant capturing nuclides. Models which allow one to estimate this radial burnout

are typically validated by mass-spectrometric analysis of a previously dissolved fraction of such material. The sampling technique necessary has to be carefully optimised in order to get a representative (normally area-averaged) analytical burnout value. In order to get a direct measure of the radial burnup of  $^{10}\text{B}$  in a hot isostatically pressed (HIPed)  $\text{B}_{8,5}\text{C}$  neutron absorber sample within the  $\text{B}_4\text{C}$  homogeneity range, a technique has been developed to analyse a sample cross-section by secondary ion mass-spectrometry (SIMS).

**2. Nuclear reactions in boron carbide**

The mean reaction with thermal neutrons is  $^{10}\text{B}(\text{n},\alpha)^7\text{Li}$  producing helium and lithium in the boron carbide matrix which induces a swelling of the material. For thermal neutrons the cross-section of this reaction is 3837 b. The cross-section for  $^{11}\text{B}$  which is about 80% of the initial boron content is about 5 mb. For the isotope  $^{12}\text{C}$  a cross-section of 3.4 mb was found [7,8]. Thus, depletion of  $^{11}\text{B}$  and  $^{12}\text{C}$  in the boron carbide matrix due to thermal neutrons can be neglected. Neutron energies in light water reactors cover the range 0.025 eV–10 MeV. Neutrons of higher energy ( $E_n > 1$  MeV) induce the reaction  $^{10}\text{B}(\text{n},2\alpha)^3\text{H}$  producing tritium and helium in the boron carbide matrix. The cross-section for neutron absorption of this reaction is 50–200 mb [9,10]. However, the tritium generating (n,2 $\alpha$ )-reaction becomes relevant above neutron energies of 1 MeV that appear in

---

\* Corresponding author. Tel.: +41-56 310 2192; fax: +41-56 310 2309.

E-mail address: olaf.gebhardt@psi.ch (O. Gebhardt).

fast breeder reactors. For high burnups of  $^{10}\text{B}$  the reactions  $^7\text{Li}(n,n'\alpha)^3\text{H}$  ( $E_n > 4$  MeV, 400 mb) and  $^7\text{Li}(n,\gamma)^8\text{Li}$  (37 mb) producing tritium, helium and lithium are also relevant [11]. However, these reactions must not be considered for the calculations of the boron burnup done in this paper.

### 3. Experimental

#### 3.1. Sample preparation

HIPed rodlets ( $\varnothing = 1.75$  mm/ $l = 10$  mm) of  $\text{B}_4\text{C}$ ,  $\text{B}_5\text{C}$ ,  $\text{B}_{6.5}\text{C}$ ,  $\text{B}_{8.5}\text{C}$  with initially natural isotopic boron content ( $80.22 \pm 0.04$  at.% of  $^{11}\text{B}$ ) were placed in the upper part of absorber rods and were irradiated for 2 yrs in a nuclear power reactor to a  $^{10}\text{B}$  depletion of nominally 55%. The integral  $^{10}\text{B}$  burnup has been calculated from standard burnup models. Cross-sections of the  $\text{B}_{8.5}\text{C}$  rodlet selected for SIMS analysis were cut in a hot cell. Then, the sample was mounted in araldite (wet) ground with diamond discs (125, 40, 20 and 10  $\mu\text{m}$ ) and polished with 3  $\mu\text{m}$  diamond paste. The sample was embedded in special specimen holders using a conductive resin and was ultrasonically cleaned in alcohol. An optical micrograph of the  $\text{B}_{8.5}\text{C}$  specimen prepared for SIMS analysis is shown in Fig. 1. The strong increase in porosity at the specimen periphery is clearly visible. A part of the specimen neighbouring to the test sample was dissolved in  $\text{Na}_2\text{CO}_3/\text{NaNO}_3$  with 10%  $\text{H}_2\text{SO}_4$  for quantitative thermion mass-spectrometry (TIMS) analysis.

#### 3.2. SEM and TIMS analyses

SEM analysis was performed with a Zeiss DSM 981 digital scanning microscope. TIMS analysis (mass 88/89,

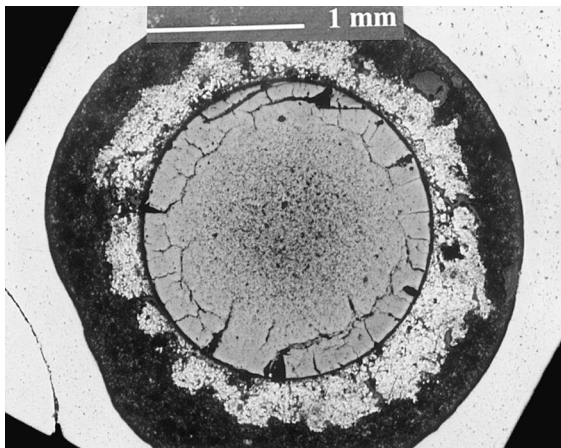


Fig. 1. Optical micrograph of the irradiated  $\text{B}_{8.5}\text{C}$  specimen prepared for SIMS analysis.

$\text{Na}_2\text{BO}_2^+$ ) using the boron standard NBS SRM 951 was performed for the quantitative determination of the average  $^{10}\text{B}/^{11}\text{B}$  ratio in the sample.

#### 3.3. Parameters for SIMS operation

The SIMS analysis was performed using a shielded Atomika Instruments S4000 secondary ion mass-spectrometer equipped with a quadrupole mass-spectrometer. Analyses were conducted for  $^7\text{Li}^+$ ,  $^{10}\text{B}^+$  and  $^{11}\text{B}^+$  secondary ions. The primary ion source was operated with  $^{133}\text{Cs}$  ions striking the samples with 11 keV at  $5^\circ$  to normal incidence. With a primary ion current of 120 nA the primary ion beam was focused down to a diameter of about 30  $\mu\text{m}$ . For analysis  $50 \times 50 \mu\text{m}^2$  areas were scanned by the primary ion beam. In order to get stable secondary ion count rates the crater was eroded away from the sample surface before performing the isotopic measurements. Images were recorded as individual depth profiles applying the motor step scan modus of the SIMS equipment. In this modus the sample stage was moved 50  $\mu\text{m}$  per step. With an image size of  $2.50 \times 2.50 \text{ mm}^2$ , 2500 individual depth profiles were recorded.

### 4. Results

#### 4.1. SEM and TIMS analyses

The SEM analysis shows typical circumferential cracks at  $r/r_0 = 0.9$ . No peripheral porosity was detected. Surface deposits were identified as P, Si and Na by additional EDX analysis in the SEM. The TIMS burnup analysis of a neighbouring sample results in an isotopic concentration of 9.77 at.% for  $^{10}\text{B}$  and 90.23 at.% for  $^{11}\text{B}$ . Thus, the average burnup of the isotope  $^{10}\text{B}$  is  $(51.0 \pm 0.5)\%$ .

#### 4.2. SIMS imaging analyses

A row area scan of the  $^7\text{Li}$ ,  $^{10}\text{B}$  and  $^{11}\text{B}$  count rates is obtained from the measurements. This direct information needed to be geometrically corrected because of problems with the movement of the sample stage which simulates an oval sample shape. Furthermore, the direct data for  $^7\text{Li}$  and  $^{10}\text{B}$  have to be normalised (presently with  $^{11}\text{B}$ ) to eliminate signal variations induced by changes of the primary ion current and distortion of the secondary ion optics due to sample stage movement. Then, a conversion of the secondary ion count rate to an isotopic surface concentration is possible.

The row area scans show a rather flat profile for lithium probably due to contamination of the sample during preparation in a wet environment. As expected from the low neutron absorption cross-section of  $^{11}\text{B}$  of

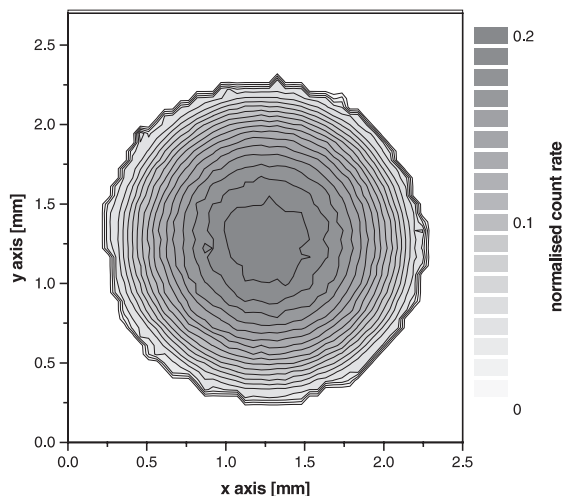


Fig. 2. Image of the normalised radial distribution of the boron isotope  $^{10}\text{B}$  versus the cross-section of the irradiated  $\text{B}_{8.5}\text{C}$  sample.

the profile, this boron isotope is sufficiently flat. Therefore, these data can be used for normalisation. The corrected and normalised area scan for the boron isotope  $^{10}\text{B}$  is presented in Fig. 2. The image shows that the burnup of the boron isotope  $^{10}\text{B}$  is relatively symmetrical. In the centre of the sample nearly the original isotopic abundance of boron has been obtained.

## 5. Discussion

Line scans can be generated from the area scans and the isotopic distribution of the two boron isotopes after irradiation can be extracted (see Fig. 3). The count rate,  $cr$  (see Eqs. (1) and (2)), of the  $^{11}\text{B}$  isotope has been used to quantify the variation of the  $^{10}\text{B}$  content after the irradiation with the assumption that the  $^{11}\text{B}$  content has not changed during irradiation. The distribution of the boron isotopic distribution ( $iso$ , Eq. (1)) and the  $^{10}\text{B}$  content and the boron burnup ( $bu$ , Eq. (2)) were calculated with (see Fig. 4)

$$\begin{aligned} iso^{10}\text{B}(r) &= \frac{cr^{10}\text{B}(r)}{cr^{10}\text{B}(r) + cr^{11}\text{B}(r)}, \\ iso^{11}\text{B}(r) &= 1 - iso^{10}\text{B}(r), \end{aligned} \quad (1)$$

$$\begin{aligned} {}^{10}\text{B}(r) &= \frac{cr^{10}\text{B}(r)}{cr^{11}\text{B}(r)} \frac{{}^{11}\text{B}_{\text{initial}}}{{}^{10}\text{B}_{\text{initial}}}, \\ bu^{10}\text{B}(r) &= 1 - {}^{10}\text{B}(r). \end{aligned} \quad (2)$$

An area averaged  $^{10}\text{B}$  burnup value was calculated and compared with the value measured by TIMS mass-spectrometry from dissolved neighbouring material. The

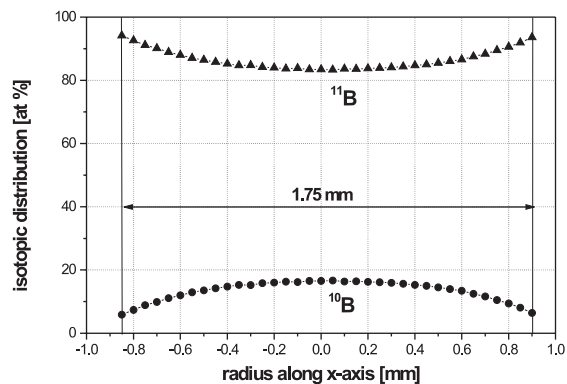


Fig. 3. Boron isotopic distribution along the  $x$ -axis.

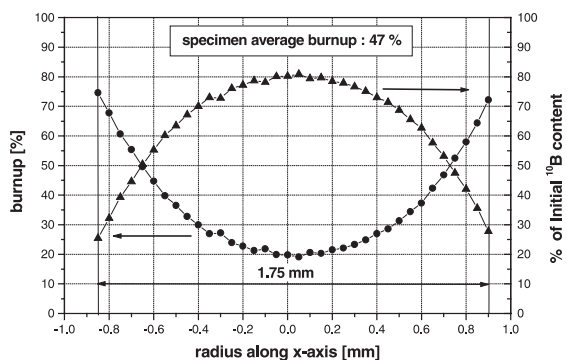


Fig. 4. Distribution of  $^{10}\text{B}$  and burnup along the  $x$ -axis.

calculated averaged burnup of the isotope  $^{10}\text{B}$  is  $(47 \pm 2)\%$ . This result is in good agreement with the result obtained by TIMS analysis  $(51.0 \pm 0.5)\%$ .

The data presented in Figs. 3 and 4 show that the applied SIMS technique leads to quantitative, local (and averaged) boron burnout results which can indeed be used to validate burnout models. The value of the technique is not limited to boron analysis but it has also been demonstrated in hafnium burnout and actinide distribution analyses on burnable poison and on  $\text{UO}_2$  and MOX fuel rods, respectively [12,13]. Obviously such analyses could be introduced also for new absorber isotopes in discussion. However, next steps should include an analysis of the helium cross-section and a normalisation of secondary ion yields using the count rates of carbon.

## 6. Conclusions

SIMS imaging analyses enable a quantitative determination of the local and average burnup of boron isotopes in boron carbide control rod samples. The de-

terminated averaged burnup of the isotope  $^{10}\text{B}$  is in good agreement with analyses by TIMS. The method of cross-sectional SIMS imaging analysis can be used to validate models which allow to calculate the  $^{10}\text{B}$  burnup in LWR control rods and to optimise new absorber materials which could be used in future (e.g. dysprosium titanate, hafnium boride, dysprosium–hafnium oxide). A verification of the profiles should occur applying the normalisation of results with the count rates of  $^{11}\text{B}$  and  $^{12}\text{C}$ .

## References

- [1] K. Reinmuth, A. Lipp, H. Knoch, J. Nucl. Mater. 124 (1984) 175.
- [2] B. Kryger, P. Herter, A. Chotard, IAEA TECDOC 813 (1995) 37.
- [3] D. Gosset, B. Kryger, IAEA TECDOC 813 (1995) 49.
- [4] B. Rebensdorf, A. Jonsson, IAEA TECDOC 813 (1995) 165.
- [5] D. Simeone, X. Deschanel, B. Berthier, C. Tessier, J. Nucl. Mater. 245 (1997) 27.
- [6] D. Simeone, D. Gosset, X. Quirion, X. Deschanel, J. Nucl. Mater. 264 (1999) 295.
- [7] A. Henglein, Einführung in die Strahlenchemie, Chemie, Weinheim, 1969.
- [8] W. Seelmann-Eggebert, G. Pfennig, H. Münzel, H. Klewe-Nebenius, Nuklidkarte, Kernforschungszentrum Karlsruhe, 1981.
- [9] E.A. Davis, F. Gabbard, T.W. Bonner, R. Bass, Nucl. Phys. 27 (1966) 462.
- [10] V. Valkovic, I. Slaus, P. Tomas, Nucl. Phys. A 98 (1967) 305.
- [11] K.K. Schnarr, thesis, Darmstadt, 1988.
- [12] H.U. Zwicky, E.T. Aerne, G. Bart, F. Patrick, H. Thomi, Radiochim. Acta 47 (1989) 9.
- [13] H.U. Zwicky, E.T. Aerne, A. Hermann, H. Thomi, M. Lippens, J. Nucl. Mater. 202 (1993) 65.